AGU PUBLICATIONS

JGR

Journal of Geophysical Research: Planets

RESEARCH ARTICLE

10.1002/2014JE004748

Key Points:
- Evolution models show that Mars' present-day Urey ratio varies by less than 10%
- Urey ratio is mainly sensitive to mantle cooling efficiency, Th, and U abundance
- Urey ratio and InSight heat flow measurement can constrain Mars' heat budget

Supporting Information:
- Figure S1

Correspondence to:
A.-C. Plesa,
Ana.Plesa@dlr.de

Citation:
Plesa, A.-C., N. Tosi, M. Grott, and D. Breuer (2015), Thermal evolution and Urey ratio of Mars, *J. Geophys. Res. Planets*, *120*, 995–1010, doi:10.1002/2014JE004748.

Received 28 OCT 2014
Accepted 11 MAR 2015
Accepted article online 16 MAR 2015
Published online 27 MAY 2015

Thermal evolution and Urey ratio of Mars

A.-C. Plesa[1], N. Tosi[1,2], M. Grott[1], and D. Breuer[1]

[1]Department of Planetary Physics, German Aerospace Center (DLR), Berlin, Germany, [2]Department of Astronomy and Astrophysics, Technische Universität Berlin, Berlin, Germany

Abstract The upcoming InSight (Interior Exploration using Seismic Investigations, Geodesy and Heat Transport) mission, to be launched in 2016, will carry out the first in situ Martian heat flux measurement, thereby providing an important baseline to constrain the present-day heat budget of the planet and, in turn, the thermal and chemical evolution of its interior. The surface heat flux can be used to constrain the amount of heat-producing elements present in the interior if the Urey ratio (*Ur*)—the planet's heat production rate divided by heat loss—is known. We used numerical simulations of mantle convection to model the thermal evolution of Mars and determine the present-day Urey ratio for a variety of models and parameters. We found that *Ur* is mainly sensitive to the efficiency of mantle cooling, which is associated with the temperature dependence of the viscosity (thermostat effect), and to the abundance of long-lived radiogenic isotopes. If the thermostat effect is efficient, as expected for the Martian mantle, assuming typical solar system values for the thorium-uranium ratio and a bulk thorium concentration, simulations show that the present-day Urey ratio is approximately constant, independent of model parameters. Together with an estimate of the average surface heat flux as determined by InSight, models of the amount of heat-producing elements present in the primitive mantle can be constrained.

1. Introduction

The heat flowing out of a planetary surface reflects the contributions of heat-producing elements (HPEs) and of the heat loss due to secular cooling. The Earth and the Moon are currently the only bodies on which in situ surface heat flux measurements have been performed. On Earth, where plate tectonics operates, the surface heat flux varies considerably with geological location. At present, it is on average 65 mW/m^2 and 100 mW/m^2 in continental and oceanic regions, respectively, but strong local variations with values up to 125 mW/m^2 can be found in volcanic regions or rift zones. Smaller variations of about 10 mW/m^2 over continents are primarily caused by the heterogeneous distribution of HPE in crustal rock [*Jaupart and Mareschal*, 2007].

The Apollo 15 and 17 missions performed measurements of the lunar surface heat flux, obtaining values of 21 and 14 mW/m^2 [*Langseth et al.*, 1976], respectively. In the absence of plate tectonics, spatial variations of the heat flux are less pronounced. However, the so-called Procellarum KREEP Terrane (PKT), where KREEP stands for potassium, rare elements, and phosphorous on the lunar nearside shows evidence for a strong enrichment in HPE [*Hubbard et al.*, 1971], and thus, the modeled present-day heat flux value in this region is as high as 34 mW/m^2 but decreases to 11 mW/m^2 for regions located far from the PKT [*Wieczorek and Phillips*, 2000]. The proximity of the Apollo 15 and 17 landing sites to the PKT thus complicates the interpretation of the measured heat fluxes. Recently, *Siegler and Smrekar* [2014] used a crustal thickness model derived from GRAIL (Gravity Recovery and Interior Laboratory) data [*Wieczorek et al.*, 2013] to obtain a mantle heat flux that can produce a surface heat flux value consistent with the measurements at both Apollo sites. Assuming a thin KREEP-rich layer to be present beneath the Apollo 15 landing site, they predicted an average mantle heat flux of 9–13 mW/m^2. These values are higher than previous estimates by *Langseth et al.* [1976] and *Wieczorek and Phillips* [2000] but similar to the results of *Warren and Rasmussen* [1987]. However, depending on the extent of the subcrustal KREEP-rich layer, i.e., whether this layer extends or not below the Apollo 17 site, the mantle heat flux can be as low as 7–8 mW/m^2 [*Siegler and Smrekar*, 2014]. Variations of the mantle heat flux of about a factor of 2 between the lunar nearside and farside may, however, be caused by an asymmetric convection structure triggered by an enriched concentration of heat sources below the PKT [*Laneuville et al.*, 2013].

The Martian surface heat flux is expected to vary less with geological location than the heat flux on the Moon. Indeed, gamma ray spectrometer data (GRS) obtained by Mars Odyssey do not present evidence for significant large-scale geochemical anomalies like the PKT [*Hahn et al.*, 2011]. The surface distribution of thorium (Th),

in contrast to the Moon where it varies by about 2 orders of magnitudes (0.1 to 12 ppm [*Taylor et al.*, 2006; *Lawrence et al.*, 2000; *Jolliff et al.*, 2000]), on Mars only shows slight variations confined between 0.2 and 1 ppm [*Taylor et al.*, 2006]. Therefore, variations in the Martian surface heat flux are expected to be mainly caused by variations in the thickness and HPE content of the crust [*Hahn et al.*, 2011] and by mantle plumes [*Kiefer and Li*, 2009; *Grott and Breuer*, 2010]. If the spatial variations are caused by differences in thickness and HPE content of the crust, the surface heat flux lies between 17 and 28 mW/m^2, while, when assuming a mantle plume underneath Tharsis, values between 15 and 60 mW/m^2 are expected [*Grott and Breuer*, 2010].

In order to obtain a first-order estimate of the overall planetary heat loss, surface heat flux has been modeled by *Grott and Breuer* [2010] using thermal evolution models based on the mantle bulk composition suggested by *Wänke and Dreibus* [1994], observed surface abundances of HPE according to *Taylor et al.* [2006], and crustal thicknesses derived from the inversion of gravity and topography data [*Neumann et al.*, 2004]. The compositional model of *Wänke and Dreibus* [1994] is based on element correlations observed in the SNC meteorites. Other models of the Martian bulk composition either derive the composition of the shergottite parent body mantle from the SNCs [*Treiman et al.*, 1986] or fit SNC oxygen isotopic composition to mixtures of chondrites [*Lodders and Fegley*, 1997]. All these models predict similar amounts of Th but substantially different potassium abundances. Another compositional model proposed by *Morgan and Anders* [1979] uses the surface ratio of K/U of 2200 as determined from gamma spectrometric analysis performed by the Soviet orbiter Mars 5, a chondritic Th/U ratio of 3.6, and constraints on the total heat output from thermal evolution models [*Toksöz and Hsui*, 1978] to estimate the absolute abundances of radiogenic heat-producing elements. This model predicts almost twice as much Th as the models of *Treiman et al.* [1986], *Wänke and Dreibus* [1994], and *Lodders and Fegley* [1997] and a significantly smaller amount of K. Currently, the most widely accepted compositional model is that of *Wänke and Dreibus* [1994], which is broadly consistent with the surface K/Th ratio measured by the GRS instrument [*Taylor et al.*, 2006]. However, heat flux estimates based on large elastic lithosphere thickness (lithospheric deflection due to loading of the north polar cap indicates present-day values larger than 300 km [*Phillips et al.*, 2008]) are significantly lower (less than 15 mW/m^2) than the average values of about 21 mW/m^2 predicted by numerical thermal evolution models that employ the bulk composition of *Wänke and Dreibus* [1994] [*Grott and Breuer*, 2010; *Morschhauser et al.*, 2011]. These thermal evolution models further predict a contribution of secular cooling to the surface heat flux of about 50% [*Breuer et al.*, 1993; *Hauck and Phillips*, 2002; *Grott and Breuer*, 2010; *Fraeman and Korenaga*, 2010; *Morschhauser et al.*, 2011]. It has thus been proposed that the HPE content of Mars' interior could be subchondritic [*Phillips et al.*, 2008] or secular cooling negligible [*Ruiz et al.*, 2011]. Nevertheless, the presence of mantle plumes beneath the Tharsis and/or Elysium provinces could cause large variations in the present-day elastic thickness of the lithosphere [*Grott and Breuer*, 2010], which, in turn, would allow evolution models based on a chondritic HPE concentration, such as that of *Wänke and Dreibus* [1994], to remain compatible with the observations.

The InSight mission (Interior Exploration using Seismic Investigations, Geodesy and Heat Transport), to be launched in 2016, will land a seismometer and a heat flux probe (HP^3) in the Elysium region of Mars and address questions related to the size, physical state, and composition of the core and mantle, thickness of the crust, and thermal state of the interior. The heat flux measurement will offer the opportunity to constrain the average Martian surface heat flux, thereby providing an independent test for the various compositional models. Assuming crustal thickness variations [e.g., *Neumann et al.*, 2004] and the surface distribution of Th and K [*Taylor et al.*, 2006; *Hahn et al.*, 2011] to be known, one can also obtain a valuable estimate of the Martian mantle heat flux by correcting the surface heat flux for the crustal contribution.

In this study, we conducted simulations of thermal evolution and investigated how the ratio between the internal heat production in the entire planet (mantle and crust) and the total surface heat loss, also termed Urey ratio (*Ur*), varies among several models of the primitive Martian mantle. It is important to note that in this study, we calculate the bulk Urey ratio, which takes into account the total heat production rate instead of the convective Urey ratio that is usually used in the literature on the Earth's thermal evolution [e.g., *Korenaga*, 2008]. Note that the latter refers to the Urey ratio calculated from the mantle abundance of radiogenic elements without the crustal contribution and from the mantle heat flux into the crust.

Table 1. Abundance of Heat-Producing Elements for Various Compositional Models and Corresponding Heat Production at the Beginning of the Evolution (H_0) and After 4.5 Ga ($H_{4.5}$)

Model	U (ppb)	Th (ppb)	K (ppm)	H_0 (pW/kg)	$H_{4.5}$ (pW/kg)
Treiman et al. [1986]	16	64	160	17	3.7
Morgan and Anders [1979]	28	101	62	21	5.8
Wänke and Dreibus [1994]	16	56	305	23	4.1
Lodders and Fegley [1997]	16	55	920	49	6.1

Running numerical models characterized by different assumptions, setups and parameter combinations, we computed the present-day value of *Ur* as

$$Ur = \frac{H\rho_{sil}V_{sil}}{F_s A_s}, \tag{1}$$

where H (in W/kg) is the interior heat production rate, F_s is the average surface heat flux, A_s is the surface area of the planet, V_{sil} is the volume of the silicate mantle shell, and ρ_{sil} its average density. Using equation (1), we can determine the interior heat production rate H knowing the average surface heat flux, which will be obtained from the measurement performed by the InSight mission. Here we identify the parameters that have a major impact on the present-day Urey ratio and discuss the implications of our results for the measurements planned in the framework of the InSight mission.

2. Models and Methods

To model the thermal evolution of terrestrial bodies, one can use either one-dimensional parametrized models or two- and three-dimensional fully dynamical simulations of mantle convection. While in the first case appropriate scaling laws are used to parametrize the convective heat transport, in the latter, the solution to the full set of conservation equations is obtained numerically. The advantage of using parametrized models is the ease with which a large parameter space can be spanned. However, albeit computationally inexpensive, such models can only provide a global, integrated picture of the interior evolution. To capture the effects associated with the spatiotemporal variability of mantle evolution, fully dynamical models are better suited. In this study, we employed the mantle convection code Gaia in 2-D cylindrical and 3-D spherical geometry [*Hüttig and Stemmer*, 2008; *Plesa*, 2011] and, to some extent, 1-D parametrized models [*Breuer and Spohn*, 2003]. We ran numerical simulations of increasing complexity and calculated the resulting present-day Urey ratio for several combinations of models and parameters. As appropriate for planetary thermal evolution, our models employ cooling boundary conditions at the core-mantle boundary (CMB) and account for the radiogenic heat production of U, Th, and K. The evolution of the CMB temperature is obtained by solving a 1-D energy equation assuming an adiabatic core with constant density and heat capacity [e.g., *Stevenson et al.*, 1983; *Steinbach and Yuen*, 1994]. We varied the initial amount of HPE according to different compositional models proposed for the interior of Mars [*Wänke and Dreibus*, 1994; *Treiman et al.*, 1986; *Morgan and Anders*, 1979; *Lodders and Fegley*, 1997] as shown in Table 1. In addition, we used various rheological formulations with which we accounted for the temperature and depth dependence of the viscosity, as well as its possible discontinuities associated with phase transitions. We varied the size of the core between 1500 and 1700 km and considered phase transitions accordingly, i.e., α to β olivine, β to γ olivine, and γ olivine to perovskite (see Table 2). In another set of models, we considered different partitioning of HPE between the mantle and a crust of constant thickness. We also tested different initial conditions (initial mantle temperature between 1650 and 1950 K and initial thermal boundary layer thickness between 50 and 300 km) and reference viscosities ranging from 10^{20} to 10^{23} Pa s, as well as various values of the activation energy between 150 and 300 kJ/mol. In all simulations we assumed a Newtonian rheology and an infinite Prandtl number, as appropriate for highly viscous media with negligible inertia. Considering the extended Boussinesq approximation (EBA) and using the mantle thickness D as length scale, the thermal diffusivity κ as time scale, and the temperature drop ΔT across the mantle as temperature scale, the nondimensional conservation equations of mass, linear momentum, and thermal energy including phase transitions, variable thermal expansivity, and conductivity read [e.g., *Christensen and Yuen*, 1985]

Table 2. Phase Transitions Parameters

Symbol	Description	Value
	Reference Depth	
$R_{\alpha\beta}$	α to β spinel	1020×10^3 m
$R_{\beta\gamma}$	β to γ spinel	1360×10^3 m
$R_{\gamma pv}$	γ spinel to perovskite	1870×10^3 m
	Density Difference $\Delta\rho$	
$\Delta\rho_{\alpha\beta}$	α to β spinel	250 kg m^{-3}
$\Delta\rho_{\beta\gamma}$	β to γ spinel	150 kg m^{-3}
$\Delta\rho_{\gamma pv}$	γ spinel to perovskite	400 kg m^{-3}
	Clapeyron Slope γ	
$\gamma_{\alpha\beta}$	α to β spinel	3×10^6 Pa
$\gamma_{\beta\gamma}$	β to γ spinel	5.1×10^6 Pa
$\gamma_{\gamma pv}$	γ spinel to perovskite	-3×10^6 Pa
	Reference Temperature	
$T_{\alpha\beta}$	α to β spinel	1820 K
$T_{\beta\gamma}$	β to γ spinel	1900 K
$T_{\gamma pv}$	γ spinel to perovskite	2000 K
w	phase transition width	20×10^3 m

$$\nabla \cdot \vec{u} = 0, \tag{2}$$

$$\nabla \cdot \left[\eta(\nabla\vec{u} + (\nabla\vec{u})^T)\right] - \nabla p + (Ra\alpha T - \sum_{l=1}^{3} Rb_l \Gamma_l)\vec{e}_r = 0, \tag{3}$$

$$\frac{DT}{Dt} - \nabla \cdot (k\nabla T) - \mathrm{Di}\alpha(T + T_0)u_r - \frac{\mathrm{Di}}{Ra}\Phi - \sum_{l=1}^{3} \mathrm{Di}\frac{Rb_l}{Ra}\frac{D\Gamma_l}{Dt}\gamma_l(T + T_0) - H = 0, \tag{4}$$

where $\vec{u}$ is the velocity vector and u_r its radial component, p the dynamic pressure, T the temperature, t the time, η the viscosity, α the thermal expansivity, k the thermal conductivity, $\vec{e}_r$ the radial unit vector, and $\Phi \equiv \tau : \dot{\varepsilon}/2$ the viscous dissipation, with τ and $\dot{\varepsilon}$ denoting the deviatoric stress and strain rate tensors, respectively. Ra is the thermal Rayleigh number, H the internal heating rate, which is given by the ratio of Ra_Q and Ra, where Ra_Q is the Rayleigh number for internal heat sources, Rb_l is the Rayleigh number associated with the deflection of the boundary of the lth phase transition, and Di is the dissipation number, given respectively by

$$Ra = \frac{\rho g \alpha \Delta T D^3}{\eta\kappa}, \quad Ra_Q = \frac{\rho^2 g \alpha H D^5}{\eta k \kappa}, \quad Rb_l = \frac{\Delta\rho_l g D^3}{\eta\kappa}, \quad \mathrm{Di} = \frac{\alpha g D}{c_p}, \tag{5}$$

where $\Delta\rho_l$ is the density jump across the lth phase transition, g the gravity acceleration, and c_p the mantle heat capacity. Phase transitions are treated as in *Christensen and Yuen* [1985] through a phase function Γ_l:

$$\Gamma_l = \frac{1}{2}\left(1 + \tanh\left(\frac{z - z_l(T)}{w}\right)\right), \tag{6}$$

where w is the phase transition width, z the depth, and $z_l(T)$ the temperature-dependent depth of phase boundaries, which is given by

$$z_l(T) = z_l^0 + \gamma_l(T - T_l^0), \tag{7}$$

where γ_l, z_l^0, and T_l^0 are the Clapeyron slope, reference transition depth, and reference transition temperature, respectively.

The viscosity is calculated according to the Arrhenius law for diffusion creep [*Karato et al.*, 1986], whose nondimensional form considering both temperature and depth dependence reads [e.g., *Roberts and Zhong*, 2006]

$$\eta(T, z) = \exp\left(\frac{E + zV}{T + T_0} - \frac{E + z_{\mathrm{ref}}V}{T_{\mathrm{ref}} + T_0}\right), \tag{8}$$

where E and V are the activation energy and volume, respectively, T_0 the surface temperature, and T_{ref} and z_{ref} the reference temperature and depth at which a reference viscosity is attained (see Table 3). In some simulations we took into account a viscosity jump of a factor of 25 in the mid-mantle as in *Roberts and Zhong* [2006], *Keller and Tackley* [2009], and, more recently, *Sekhar and King* [2014].

In some models we also considered a temperature- and pressure-dependent thermal expansivity for which we used the parametrization suggested by *Tosi et al.* [2013a]:

$$\alpha(T, z) = \left(a_0 + a_1 T + a_2 T^{-2}\right)\exp(-a_3 z); \tag{9}$$

where a_0, a_1, a_2, and a_3 are numerical coefficients appropriate for forsterite obtained by fitting results of first-principles simulations to the above equation [*Tosi et al.*, 2013a]. All variables and parameters used in equations (2)–(8) are listed in Tables 1–4.

Table 3. Parameters Held Constant in All Simulations

Symbol	Description	Value
R_p	Planetary radius	3400×10^3 m
ΔT	Temperature drop across the mantle	2000 K
T_0	Surface temperature	250 K
T_{ref}	Reference temperature	1600 K
E	Activation energy	3×10^5 J mol^{-1}
V	Activation volume	6×10^{-6} m^3 mol^{-1}
c_p	Mantle heat capacity	1200 J kg^{-1} K^{-1}
ρ	Mantle density	3500 kg m^{-3}
ρ_{cr}	Crust density	2900 kg m^{-3}
c_c	Core heat capacity	850 J kg^{-1} K^{-1}
ρ_c	Core density	7000 kg m^{-3}
g	Gravity acceleration	3.7 m s^{-2}
k	Mantle thermal conductivity	4 W m^{-1} K^{-1}
κ	Mantle thermal diffusivity	1×10^{-6} m^2 s^{-1}

3. Results

3.1. Reference Viscosity and Thermostat Effect

In this first set of models, we investigated the effects of the mantle cooling efficiency on the Urey ratio assuming the Boussinesq approximation and temperature-dependent viscosity. The influence of depth-dependent viscosity, extended Boussinesq approximation, phase transitions, and various partitioning of heat-producing elements between mantle and a low-conductivity crust on the results are discussed in section 3.3. In Figure 1 we show the evolution of the Urey ratio and mean surface heat flux obtained from 2-D models in which we assumed a heat production rate according to the compositional model of *Wänke and Dreibus* [1994] and varied the mantle reference viscosity between 10^{20} and 10^{23} Pa s, the initial mantle temperature between 1650 and 1950 K, the initial thickness of both the upper and lower thermal boundary layers (TBL) between 50 and 300 km, and the activation energy between 150 and 300 kJ/mol. The temperature dependence of the viscosity is responsible for a thermostat effect that regulates the state of the interior in such a way that initial conditions only exert a relatively weak influence on the present-day thermal state of the planet. In particular, for high initial temperatures, viscosity is reduced, convective vigor is high, and the mantle tends to cool at a relatively fast rate. On the contrary, low initial temperatures result in large viscosities, slow convection, and slow cooling. Figures 1a and 1b clearly show that this mechanism works efficiently as long as the reference viscosity is lower than 10^{22} Pa s. In such a case, the present-day Urey ratio and mean surface heat flux lie around 0.54 and 26 mW/m^2, respectively. The Urey ratio varies within 1.6% assuming $\eta_{ref} = 10^{21}$ Pa s and different initial temperatures (Figures 1c and 1d) or $\eta_{ref} = 10^{21}$ Pa s and different values of the activation energy (Figures 1e and 1f).

We also carried out the same simulations using 1-D parametrized models (see supporting information Figure S1). These models show a very similar behavior: the surface heat flow and hence the Urey ratio converge both toward a present-day value of 22 mW/m^2 and 0.63, respectively, independent of the input parameters. It should be also noted that despite the use of the same parameters, the parametrized models predict

Table 4. Parameters Varied Among Different Simulations

Symbol	Description	Value
R_c	Core radius	1500×10^3, 1700×10^3 m
D	Mantle thickness	1900×10^3, 1700×10^3 m
α	Reference thermal expansivity	2.5×10^{-5}, 4.26×10^{-5} K^{-1}
η	Reference viscosity	10^{20}–10^{23} Pa s
Q_m	Initial amount of radiogenic heating	17×10^{-12}–49×10^{-12} W kg^{-1}
Ra	Thermal Rayleigh number	3.18×10^6–4.44×10^6
Ra_Q	Internal heat sources Rayleigh number	9.25×10^7–1.61×10^8
Di	Dissipation number	0.223–0.146
k_{cr}	Crust thermal conductivity	2, 3 W m^{-1} K^{-1}

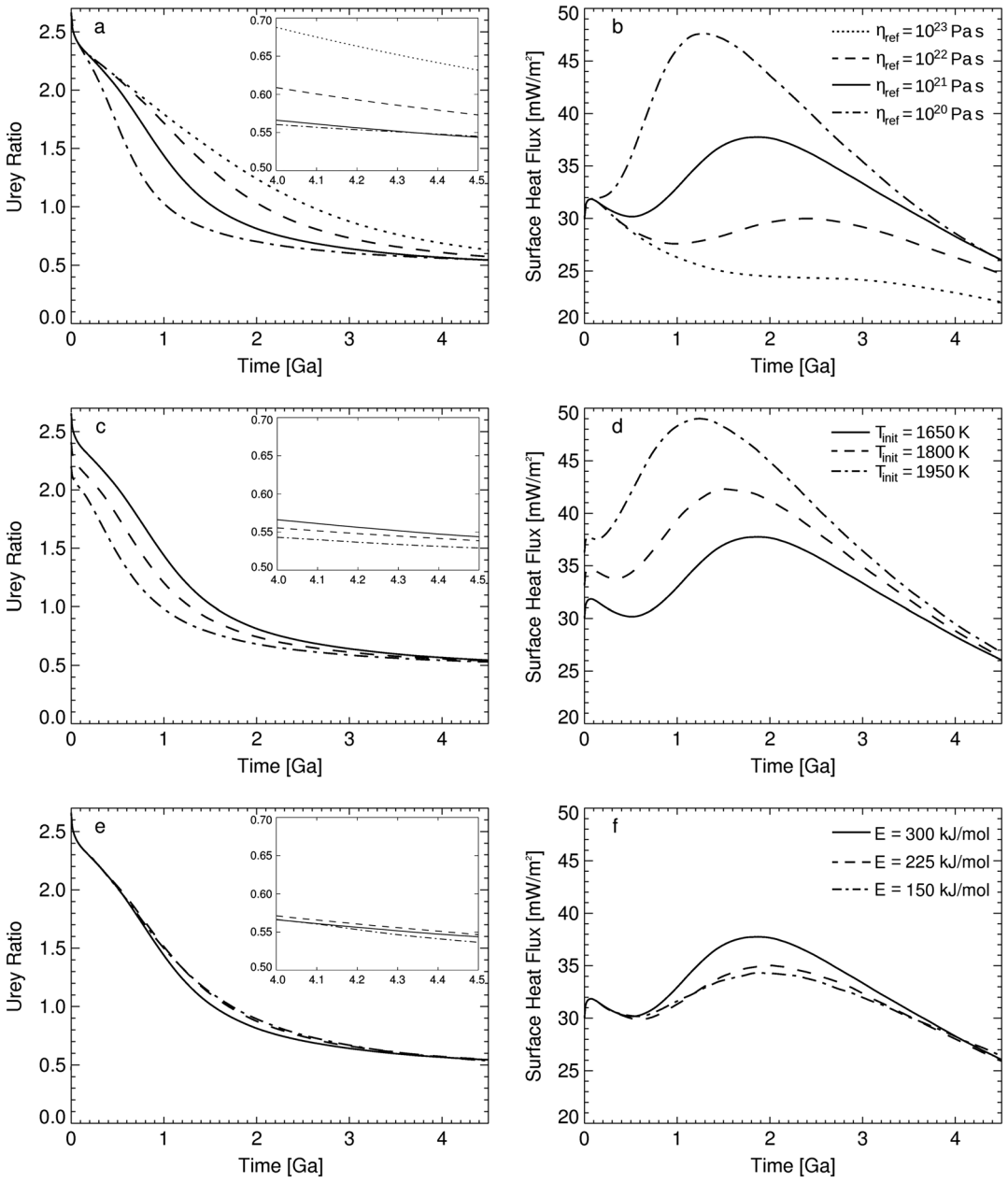

Figure 1. Thermostat effect: (a, c, and e) Urey ratio and (b, d, and f) surface heat flux for reference viscosities from 10^{20} to 10^{23} Pa s (Figures 1a and 1b and cases 1–3 and 5 in Table 5), initial mantle temperatures from 1650 to 1950 K (Figures 1c and 1d and cases 3, 14, and 15), and activation energy from 150 to 300 kJ/mol (Figures 1e and 1f and cases 3, 20, and 21). The inset in Figures 1a, 1c, and 1e shows the Urey ratio during the last 500 Ma of evolution.

present-day Urey ratios that are systematically higher than those computed with 2-D or 3-D dynamic simulations (approximately by 0.1). The reason is likely a simplification made in our 1-D models. In fact, the time dependence present in the diffusion equation that is solved to determine the temperature in the stagnant lid is neglected under the assumption of steady state conduction [see, e.g., *Morschhauser et al.*, 2011, equation (5)]. The absence of this term causes the stagnant lid to grow more rapidly than it should with the consequence that the surface heat flux tends to be relatively small, eventually leading to a slight overestimation of the Urey ratio. Nevertheless, the fact that the Urey ratio remains largely unaffected by the choice of different input parameters is a robust result, clearly unrelated to the use of parametrized models, which generally deliver global solutions that match very well with dynamic ones [*Tosi et al.*, 2013b].

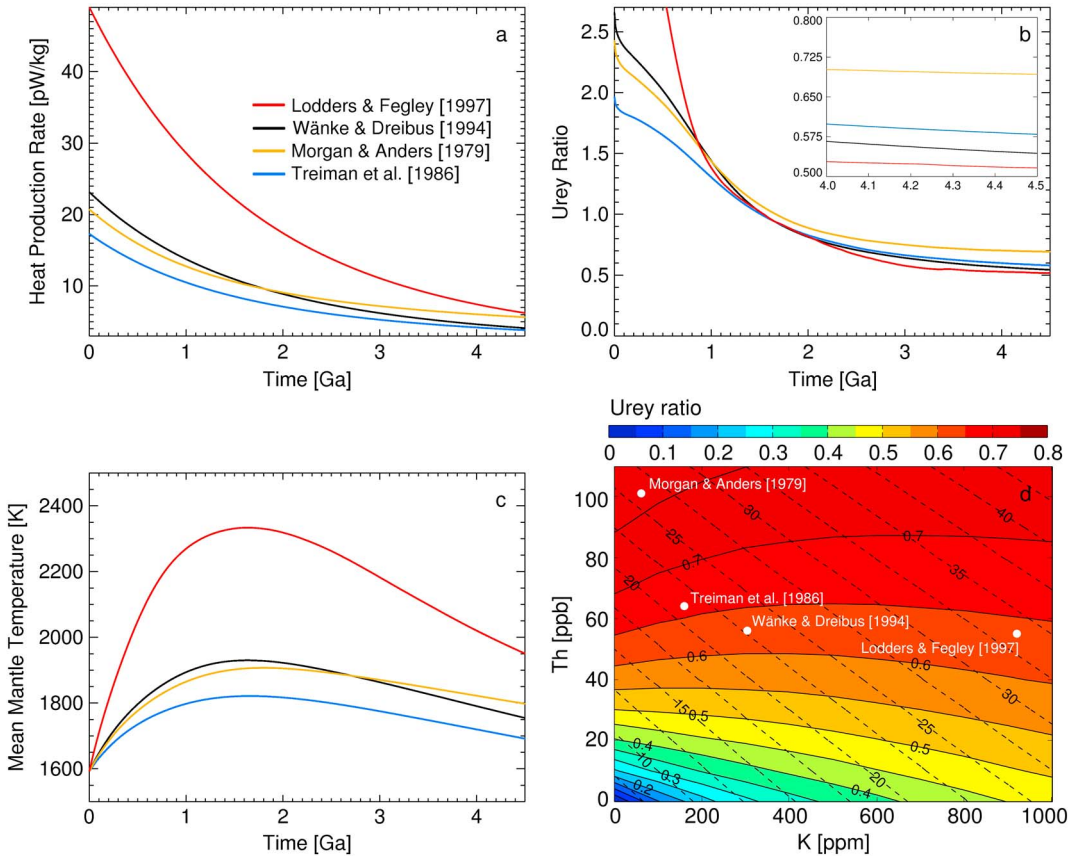

Figure 2. Effect of different HPE models: (a) heat production as a function of time for the four compositional models considered, (b) corresponding Urey ratio obtained using a reference viscosity of 10^{21} Pa s (cases 3 and 11–13 in Table 5), (c) time evolution of the mean mantle temperature, and (d) map of the Urey ratio (solid lines) and surface heat flux in mW/m^2 (dashed lines) as function of Th and K content obtained from 1-D parametrized models (white circles correspond to the HPE concentrations of the four models of Figure 2a).

3.2. Mean Half-Life of Radiogenic Isotopes

To calculate the effects of various HPE models on the Urey ratio, we ran simulations in which we assumed bulk compositions derived from *Wänke and Dreibus* [1994], *Treiman et al.* [1986], *Morgan and Anders* [1979], and *Lodders and Fegley* [1997] (Figure 2a and Table 1) and a reference viscosity of 10^{21} Pa s. With the exception of *Morgan and Anders* [1979], all other models are characterized by similar concentrations of Th and U (i.e., 55–64 ppb and 16 ppb, respectively), with Th/U ratios limited between 3.5 and 4, but remarkably different concentrations of K, the highest of which (920 ppm) is predicted by *Lodders and Fegley* [1997] (Table 4). When using the latter model, during the first half of the evolution, the mantle temperature can become up to 500 K higher than that obtained using the other compositional models (Figure 2c). Although this difference decreases during the thermal evolution, the present-day mean mantle temperature is more than 300 K higher compared to other compositional models. Because of the relatively short half-life of K (1.25 Ga), the Urey ratio tends to be anomalously large at the beginning of the evolution. However, after about 1 Ga, it rapidly converges to values similar to those obtained when assuming different HPE concentrations and remains close to them until present (Figure 2b). The high Th and U content that characterizes the model of *Morgan and Anders* [1979] has a strong influence on the evolution of the Urey ratio and its present-day value. After the initial heating phase, the mantle cools very slowly, leading to a Urey ratio systematically higher (by at least 16.8%) than that obtained in the other cases.

In order to investigate in more detail the effects of different HPE concentrations, we carried out a large number of simulations based on 1-D parametrized models. Figure 2d shows a contour plot of the present-day Urey ratio as a function of the concentration of Th and K for a constant Th/U ratio of 3.5. The white circles refer to the four HPE models that we considered. While the present-day *Ur* only weekly depends on the abundance of K, which mainly influences the early evolution of the planet, it varies considerably in dependence of the

Table 5. Results of All Presented 2-D and 3-D Simulations[a]

Case	Geometry	Features	*Ur*	F_s [Min, Max] (mW/m^2)	F_{cmb} (mW/m^2)	T_{mean} (K)	T_{cmb} (K)
Reference Viscosity (HPE = Wae, $\eta(T)$, D_l = 300 km, T_{init} = 1650 K)							
1	2-D	$\eta_{ref} = 10^{23}$ Pa s	0.631	22.03 [21.76, 22.46]	0.14	1940.58	2300.84
2	2-D	$\eta_{ref} = 10^{22}$ Pa s	0.572	24.71 [23.88, 25.64]	2.90	1865.80	2163.67
3	2-D	$\eta_{ref} = 10^{21}$ Pa s	0.543	26.03 [25.31, 26.79]	3.80	1754.51	1996.87
4	3-D	$\eta_{ref} = 10^{21}$ Pa s	0.570	24.84 [24.34, 25.37]	2.36	1720.09	1981.11
5	2-D	$\eta_{ref} = 10^{20}$ Pa s	0.545	25.97 [25.09, 26.93]	4.15	1632.07	1833.26
HPE Models ($\eta_{ref} = 10^{22}$ Pa s, $\eta(T)$, D_l = 300 km, T_{init} = 1650 K)							
6	2-D	HPE = Mor	0.740	26.72 [26.07, 27.92]	1.00	1909.35	2180.04
7	2-D	HPE = Tre	0.627	20.71 [20.26, 21.30]	2.19	1776.51	2101.86
8	2-D	HPE = Lod	0.533	40.44 [38.83, 42.59]	7.07	2113.15	2348.60
HPE Models ($\eta_{ref} = 10^{20}$ Pa s, $\eta(T)$, D_l = 300 km, T_{init} = 1650 K)							
9	2-D	HPE = Mor	0.683	28.91 [27.79, 29.84]	3.19	1674.35	1855.62
10	2-D	HPE = Tre	0.566	22.93 [22.30, 23.66]	2.89	1586.06	1800.79
HPE Models and Initial Temperature ($\eta_{ref} = 10^{21}$ Pa s, $\eta(T)$, D_l = 300 km, T_{init} = 1650 K[a], T_{init} = 1800 K[b], T_{init} = 1950 K[c])							
11	2-D	HPE = Mor[a]	0.692	28.55 [27.57, 29.78]	3.35	1797.84	2018.61
12	2-D	HPE = Tre[a]	0.579	22.44 [21.87, 23.20]	3.43	1691.66	1953.12
13	2-D	HPE = Lod[a]	0.516	41.78 [40.42, 43.37]	2.97	1950.47	2119.36
14	2-D	HPE = Wae[b]	0.538	26.28 [25.53, 27.17]	1.60	1755.77	1979.57
15	2-D	HPE = Wae[c]	0.529	26.76 [25.98, 27.65]	1.57	1762.84	1984.80
16	2-D	HPE = Tre[c]	0.549	23.68 [23.14, 24.35]	1.52	1709.57	1948.08
17	2-D	HPE = Mor[c]	0.660	29.95 [29.15, 30.97]	3.30	1818.96	2036.53
Initial TBL (D_l) (HPE = Wae, $\eta_{ref} = 10^{21}$ Pa s, $\eta(T)$, T_{init} = 1650 K)							
18	2-D	D_l = 50 km	0.552	25.64 [24.87, 26.37]	1.22	1746.04	1972.92
19	2-D	D_l = 175 km	0.550	25.71 [24.89, 27.09]	1.56	1746.07	1972.53
20	2-D	E = 150 kJ/mol	0.536	26.38 [25.55, 27.47]	2.27	1766.72	2002.68
21	2-D	E = 225 kJ/mol	0.546	25.91 [25.25, 27.22]	1.86	1762.82	1996.41
Depth Dependence of the Viscosity (HPE = Wae, $\eta_{ref} = 10^{21}$ Pa s, $\eta(T,p)$, T_{init} = 1650 K)							
22	2-D		0.546	25.92 [23.43, 31.24]	4.19	1739.50	2054.02
23	2-D	D_c = 1500 km	0.543	27.17 [23.49, 32.31]	1.39	1771.36	2028.35
24	3-D		0.575	24.60 [22.80, 28.85]	3.73	1699.11	2042.27
25	2-D	$\Delta\eta_{jump} = 25$	0.560	25.25 [21.58, 37.35]	1.64	1733.83	2114.94
26	3-D	$\Delta\eta_{jump} = 25$	0.581	24.35 [20.21, 37.43]	3.28	1695.77	2137.40
Adiabatic Heating and Cooling ($\eta_{ref} = 10^{21}$ Pa s, $\eta(T,p)$, T_{init} = 1650 K, EBA, HPE = Wae (W), HPE = Tre (T))							
27	2-D	(W)	0.564	25.09 [22.68, 26.97]	4.10	1806.26	2236.99
28	2-D	$\alpha(T,p)$, (W)	0.578	24.49 [23.68, 25.64]	2.02	1804.84	2302.08
29	2-D	(T)	0.614	21.17 [20.05, 22.70]	1.36	1739.40	2169.85
Phase Transitions (HPE = Wae, $\eta_{ref} = 10^{21}$ Pa s, $\eta(T,p)$, T_{init} = 1650 K, EBA, PT)							
30	2-D		0.563	25.14 [24.10, 26.47]	1.61	1808.52	2209.18
31	3-D		0.594	23.82 [22.64, 24.79]	3.31	1767.81	2207.27
32	2-D	D_c = 1500 km	0.554	26.62 [24.92, 28.47]	1.41	1855.73	2264.25
33	3-D	D_c = 1500 km	0.602	24.50 [23.52, 26.59]	3.08	1799.04	2261.07
34	2-D	$\alpha(T,p)$	0.572	24.71 [24.03, 25.54]	1.67	1810.35	2301.95
35	3-D	$\alpha(T,p)$	0.618	22.90 [22.37, 23.41]	2.82	1760.37	2283.93

concentration of Th. The Urey ratios obtained when using the HPE models of *Wänke and Dreibus* [1994], *Lodders and Fegley* [1997], and *Treiman et al.* [1986], which are all characterized by similar amounts of Th, lie within a narrow range of ~0.05. The use of the model by *Morgan and Anders* [1979], which predicts about twice as large a concentration of Th, leads instead to a significantly higher Urey ratio (more than 16.8% higher compared to the other compositional models).

Table 5. (continued)

Case	Geometry	Features	*Ur*	F_s [Min, Max] (mW/m^2)	F_{cmb} (mW/m^2)	T_{mean} (K)	T_{cmb} (K)
Thermal Conductivity of the Crust (HPE = Wae, $\eta_{ref} = 10^{21}$ Pa s, $\eta(T,p)$, $T_{init} = 1650$ K, EBA, PT, $Q_{cr} = 49$ pW/kg)							
36	2-D	$k_{cr} = 2$ W/m K	0.571	24.78 [21.24, 29.07]	1.12	1725.68	2101.49
37	3-D	$k_{cr} = 2$ W/m K	0.591	23.93 [21.12, 27.04]	2.79	1700.43	2120.41
38	2-D	$k_{cr} = 3$ W/m K	0.569	24.84 [20.88, 29.25]	1.02	1727.26	2107.15
Present-Day HPE Enrichment in the Crust (HPE = Wae, $\eta_{ref} = 10^{21}$ Pa s, $\eta(T,p)$, $T_{init} = 1650$ K, EBA, PT, $k_{cr} = 2$ W/m K)							
39	2-D	*Q* uniform	0.557	25.42 [23.23, 28.87]	2.04	1860.42	2200.96
40	2-D	$Q_{cr} = 25$ pW/kg	0.537	26.33 [21.67, 32.01]	1.51	1720.19	2051.72
41	2-D	$Q_{cr} = 32$ pW/kg	0.561	25.23 [21.20, 32.31]	1.32	1700.65	2046.03
42	2-D	$Q_{cr} = 62$ pW/kg	0.572	24.72 [19.46, 36.48]	0.39	1623.11	2008.75
43	2-D	$Q_{cr} = 75$ pW/kg	0.577	24.53 [19.49, 35.83]	0.49	1574.55	1970.23
44	2-D	$Q_{cr} = 100$ pW/kg	0.555	25.46 [19.76, 31.41]	0.76	1476.13	1912.73
45	2-D	$Q_{cr} = 110$ pW/kg	0.528	26.82 [19.88, 33.74]	1.02	1385.26	1830.04

[a] All values refer to present day. *Ur*: Urey ratio, F_s [min, max]: surface heat flux with its minimum and maximum values, F_{cmb}: CMB heat flux, T_{mean}: mean mantle temperature, and T_{cmb}: CMB temperature. The parameter Q_{cr} indicates the present-day HPE in the crust, with $Q_{cr} = 49$ pW/kg being the present-day average based on the GRS data [*Hahn et al.*, 2011].

In addition, we varied the Th/U ratio between 2 and 5 to test the sensitivity of our results to these parameters, even though it is important to point out that typical solar system and terrestrial Th/U ratios have been estimated to be confined within a narrow range of about 3.9 ± 0.2 [e.g., *Rocholl and Jochum*, 1993]. With Th/U ratios between 3.5 and 4, as predicted by the four compositional models that we considered (Table 1), the variations in the present-day Urey ratio are within ~0.79%. However, considering a broader range of Th/U ratios between 2 and 5 leads to variations in the present-day *Ur* as large as 5.68%.

3.3. Additional Effects

In order to assess the robustness of our result regarding the prediction of a constant present-day Urey ratio, we conducted a series of simulations in which we took into account a number of additional complexities. Specifically, we considered different core sizes, phase transitions, different rheological formulations (namely, temperature-dependent viscosity, temperature- and depth-dependent viscosity, and including an additional viscosity jump in the mid-mantle), and partitioning of HPE between mantle and crust. All these cases have been examined assuming the compositional model of *Wänke and Dreibus* [1994]. The corresponding results are listed in Table 5, and some of the models are shown in Figures 3– 5. The Urey ratio resulting from our simulations is 0.565 ± 0.049 for 2-D models and 0.594 ± 0.024 for 3-D models, corresponding to an uncertainty smaller than 10%.

3.3.1. Depth Dependence of the Viscosity

We first investigated the effects on the surface heat flux and present-day Urey ratio assuming various viscosity formulations as proposed in the literature for the Martian mantle. The use of a purely temperature-dependent viscosity results in a small-scale convection pattern (Figure 3a). Accounting for a strong pressure dependence of the viscosity tends to cause the formation of a low-degree pattern that may result in a degree-one convection structure (Figure 3b). An additional viscosity jump in the mid-mantle favors a one-ridge convection structure as previously observed by *Keller and Tackley* [2009] (Figure 3c). The convection planforms shown in Figure 3 all refer to present-day snapshots obtained using the various viscosity formulations mentioned above. Although in a single model the difference between minimum and maximum surface heat flux can be as large as 15 mW/m^2, all models are characterized by a very similar average surface heat flux of about 24.5 mW/m^2.

In Figure 4 we show the evolution of average quantities for the above cases from simulations conducted both in 2-D and 3-D geometry. Although the difference in the present-day mean mantle and CMB temperatures among the various models amounts to 20 and 60 K, respectively, and the convection pattern changes considerably (Figure 3), the present-day mean surface heat flux varies by less than 1 mW/m^2, which causes only a minor variation in the present-day Urey ratio (less than 10%). Also note that 2-D models lead to slightly smaller Urey ratios than 3-D models (Figure 4a).

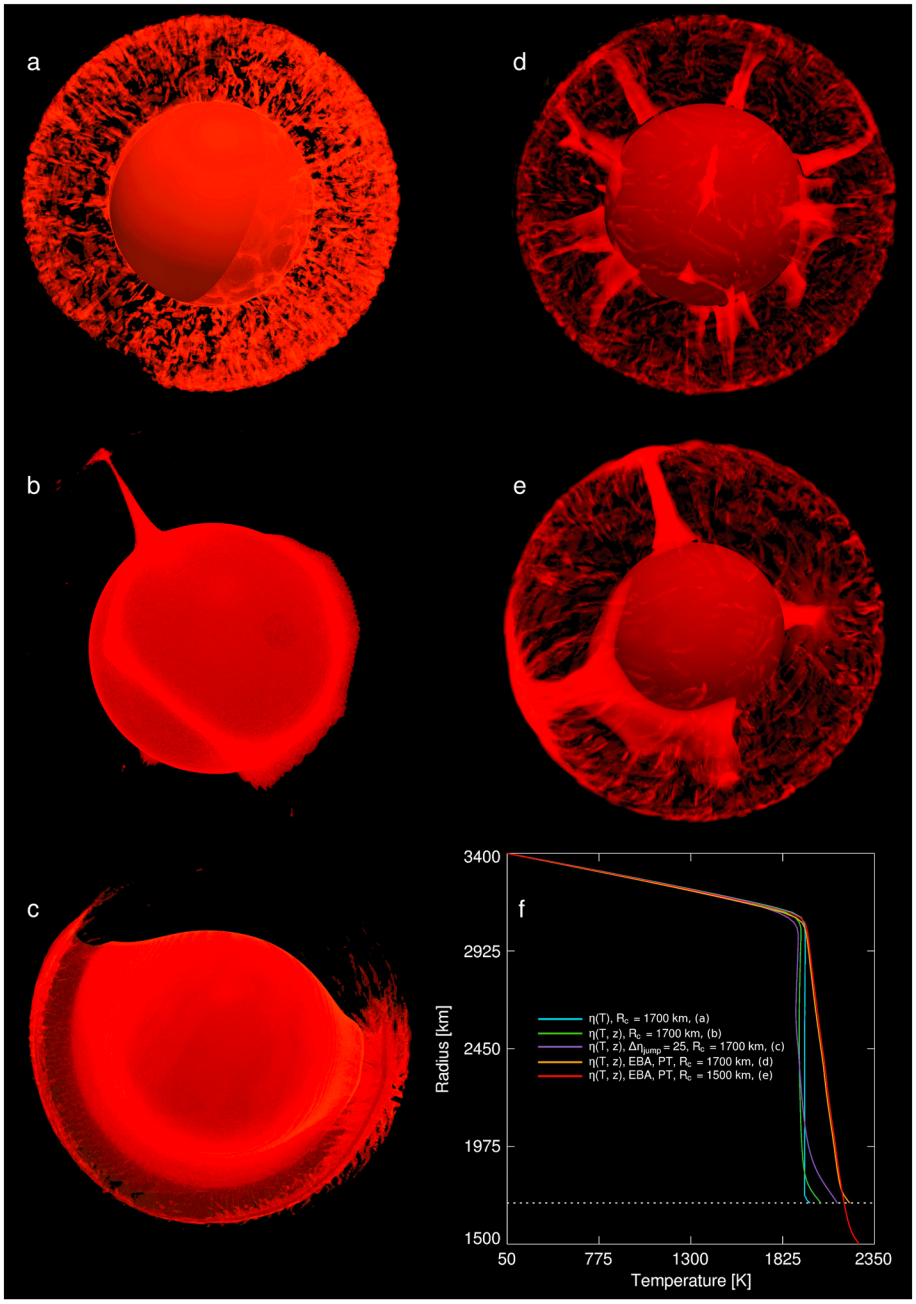

Figure 3. Additional effects: temperature distribution after 4.5 Ga of evolution for a simulation with (a) temperature-dependent viscosity and a core size of 1700 km (case 4); (b) temperature- and depth-dependent viscosity and a core size of 1700 km (case 24); (c) temperature- and depth-dependent viscosity, a 25-fold viscosity jump in the mid-mantle, and a core size of 1700 km (case 26); (d) temperature- and depth-dependent viscosity, phase transitions, and a core size of 1700 km (case 31); (e) temperature- and depth-dependent viscosity, phase transitions, and a core size of 1500 km (case 33); and (f) corresponding temperature profiles.

3.3.2. Adiabatic Heating and Cooling

We run additional simulations where we took into account adiabatic heating and cooling by using the EBA and a temperature- and pressure-dependent thermal expansion coefficient $\alpha(T, p)$. The present-day average surface heat flux and hence the Urey ratio have values similar to those obtained from the models discussed above, although the mean mantle temperature and CMB temperature differ by 60 K and 250 K, respectively (compare models 20, 24, and 25 in Table 5). Moreover, cases that account for adiabatic heating and cooling are characterized by smaller surface heat flux variations (less than 5 mW/m^2) when compared to Boussinesq cases when using the same CMB temperature of 2250 K. The use of the EBA results in a smaller temperature

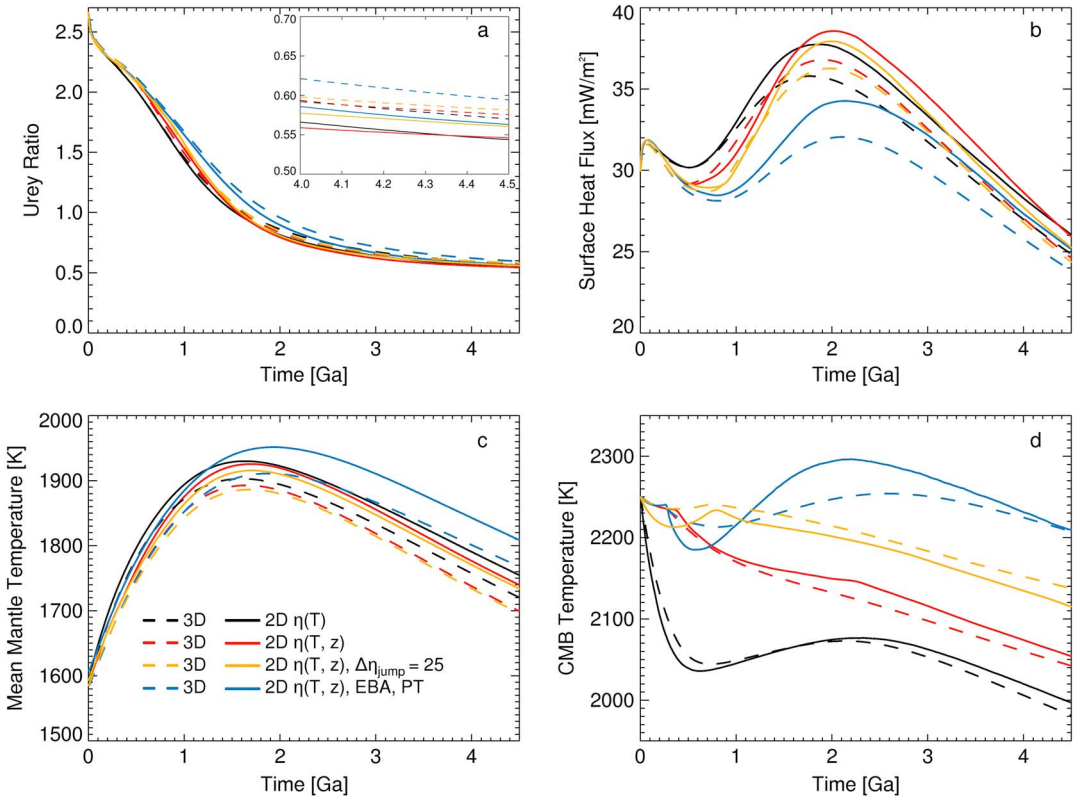

Figure 4. Additional effects: time evolution of (a) Urey ratio, (b) surface heat flux, (c) mean mantle temperature, and (d) CMB temperature for various 2-D (full lines) and 3-D (dashed lines) models using only temperature-dependent viscosity (black lines, cases 3 and 4, respectively); temperature- and depth-dependent viscosity (red lines, cases 22 and 24, respectively); an additional viscosity jump in the mid-mantle (yellow lines, cases 25 and 26, respectively); and EBA and phase transitions (blue lines, cases 30 and 31, respectively).

drop across the bottom thermal boundary layer. This causes the emergence of plumes with lower excess temperatures that ultimately lead to reduced spatial variations of the surface heat flux compared to cases based on the Boussinesq approximation (compare orange and green lines in Figure 3f). It should be noted that in the framework of the extended Boussinesq approximation, we also tested the influence of using a larger initial temperature jump across the CMB in order to correct for adiabatic effects. Also in this case, we found that

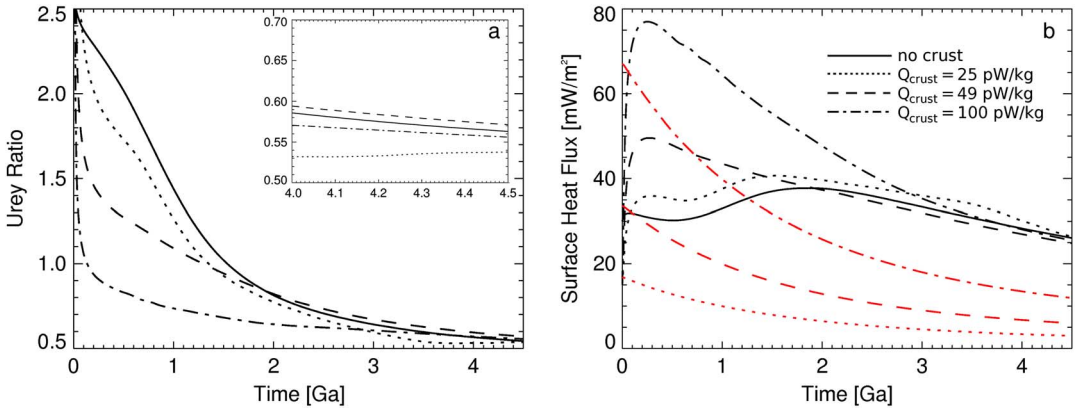

Figure 5. Effects of the crust: time evolution of (a) Urey ratio and (b) surface heat flux (black lines) and crustal contribution (red lines) for different HPE enrichment factors between mantle and crust chosen in such a way that the present-day amount of HPE in the crust is either 25 (dotted line, case 40), 49 (dashed line, case 36), or 100 pW/kg (dash-dotted line, case 44). An additional case is shown where no partitioning of HPE was used (full line, case 3).

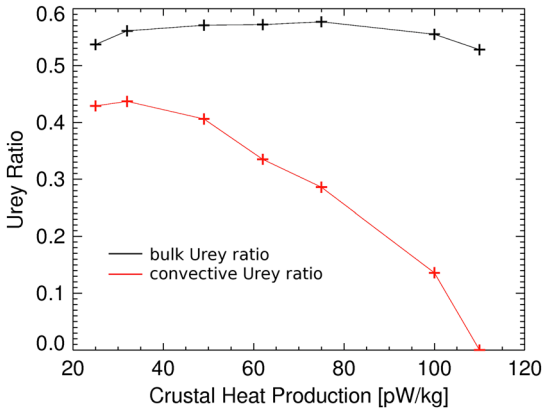

Figure 6. Bulk and convective Urey ratios (see section 1 for their definition) as a function of the crustal heat production for models including EBA, phase transitions, and a crust thermal conductivity of 2 W/mK (cases 36 and 40–45). While the bulk Urey ratio remains nearly constant upon varying the concentration of HPE in the crust, the convective Urey ratio changes considerably. A Urey ratio of 0 corresponds to a situation in which the mantle is fully depleted in HPE, which are concentrated solely in the crust.

spatial variations of the heat flux remain small when compared to those obtained from simulations based on the Boussinesq approximation.

3.3.3. Phase Transitions

The snapshots shown in Figures 3d and 3e also take into account non-Boussinesq effects through the EBA. In addition, depending on the size of the core, either two exothermic (for a core radius of 1700 km, Figure 3b) or two exothermic and one endothermic (for a core radius of 1500 km, Figure 3d) phase transitions are considered (see Table 2). As expected, the simulation with a smaller core size results in a convection structure characterized by a pattern with longer wavelength than that obtained in the simulation with a 200 km larger core radius. Nevertheless, this has again little influence on the structure of the upper thermal boundary layer and hence on the average heat flux (Figure 3f).

3.3.4. HPE Enrichment in the Crust

In this final set of simulations, we assumed an initial radiogenic heat budget of $\sim$ 11.6 TW for the interior according to *Wänke and Dreibus* [1994]. We varied the amount of heat-producing elements in the crust in order to obtain a present-day crustal heat production of 25, 49, 75, or 100 pW/kg. We kept the thickness of the crust fixed over the entire thermal evolution, but we also included lateral variations in order to mimic the effects of the southern highlands and northern lowlands, for which we assumed crustal thicknesses of 60 and 30 km, respectively. In addition, we used a thermal conductivity of either 2 W/m K or 3 W/m K in the crust and of 4 W/m K in the mantle (Tables 3 and 4).

The amplitude of the temperature gradient at the surface increases when considering a crust with constant thickness, enriched in HPE, and having a lower thermal conductivity with respect to the mantle. However, the average surface heat flux remains similar to that obtained from the simulations in which crustal effects are not taken into account as a consequence of the reduced thermal conductivity and also because the mantle contribution to the surface heat flux is controlled both by the thermal conductivity and by the amount of radiogenics contained in the crust (Figure 5b). In conclusion, also these models are characterized by a similar present-day bulk Urey ratio, although the convective Urey ratio varies significantly (Figure 6).

4. Discussion

Our models demonstrate that for a one-plate planet like Mars, variations of the present-day bulk Urey ratio lie within about 10%. On the base of the values reported in Table 5 and considering only simulations with a reference viscosity of 10^{21} Pa s or smaller as suggested by previous studies of the evolution of Mars' mantle [e.g., *Grott and Breuer*, 2008; *Morschhauser et al.*, 2011], we find, for the 2-D cylindrical models, $Ur = 0.565 \pm 0.049$ (i.e., Ur lies between 0.516 and 0.614). The 3-D spherical simulations lead to slightly higher values, with $Ur = 0.594 \pm 0.024$ (i.e., between 0.57 and 0.618). In contrast, estimates of the present-day convective Urey ratio for the Earth vary more significantly (by a factor of 2 or even more), likely because of additional complexities due to plate tectonics, melt generation, and the presence of continents [e.g., *Korenaga*, 2006; *Jaupart and Mareschal*, 2007; *Butler*, 2009; *Lenardic et al.*, 2011; *Nakagawa and Tackley*, 2012]. In fact, a recent study shows that for the Earth the Urey ratio can vary considerably depending on the amount of internal heat production, while similar values for the present-day surface heat flux are obtained [*Nakagawa and Tackley*, 2012]. In this study it has also been shown that magmatic heat transport is an important contributor to the planetary heat loss. The effects of this process are particularly important during the early evolution, when a large amount of melt is produced. However, for the Earth, magmatism associated with mantle upwellings can still affect considerably the present-day surface heat flux [*Nakagawa and Tackley*, 2012].

For Mars instead, the effects of magmatic heat transport on the present-day surface heat flux are negligible, since no large amounts of melt are expected to be produced in the interior. The absence of a mobile surface

and of continents also simplifies the system. Our simulations indeed show that the Urey ratio is mainly sensitive to the efficiency of mantle cooling, which chiefly depends on the mantle viscosity and on the absolute abundance of long-lived radiogenic isotopes, particularly of Th and U. Using solar system values for the Th/U ratio, variations of the Urey ratio lie within 2%. Our models show that the thermostat effect is efficient for reference viscosities smaller than 10^{22} Pa s, a situation that may be well representative of Mars' mantle. In fact, previous studies suggest that a low-reference mantle viscosity is better suited to match observational constraints related to the thickness of the elastic part of the lithosphere and of the crust [e.g., *Grott and Breuer*, 2008; *Morschhauser et al.*, 2011]. The presence of a significant amount of water in some shergottite magmas [*McCubbin et al.*, 2012] also indicates that a wet mantle rheology with reference viscosities as low as 10^{19} Pa s is to be expected. Under these circumstances, variations of the Urey ratio caused by different initial conditions vanish within ~3 Ga of evolution at the latest, due to the high efficiency of the thermostat effect.

When modeling the dynamics and thermal evolution of the interior, the least constrained parameter is the rheology, which we widely varied by testing various reference viscosities, initial mantle temperatures, viscosity variations with depth, and activation energies. Although our simulations were performed assuming a Newtonian rheology, in some of the tests we used a lower activation energy (cases 20 and 21 in Table 5), which has been argued to mimic the effects of the nonlinear rheology associated with dislocation creep [*Christensen*, 1984]. These tests show Urey ratios that are very similar to those obtained when using an activation energy of 300 kJ/mol, representative of the Newtonian rheology associated with diffusion creep.

It is important to note that the bulk Urey ratio is independent of the distribution of radioactive elements between mantle and crust. In contrast, the convective Urey ratio decreases with increasing enrichment of radiogenics into the crust. We also calculated the Urey ratio using parametrized models with a reference viscosity of 10^{18} Pa s, a self-consistent treatment of the crust production, and dehydration stiffening as in *Morschhauser et al.* [2011] and found variations of only few percent with respect to the values predicted by the parametrized models used in this study (Figure 2). Moreover, the Urey ratio from fully 2-D dynamic models that develop a layered convection structure resulting from the self-consistent treatment of crust production and mantle depletion [*Plesa and Breuer*, 2014] varies between 0.575 and 0.607 and is thus similar to the values presented in this work.

The HPE models of *Wänke and Dreibus* [1994], *Treiman et al.* [1986], and *Lodders and Fegley* [1997], derived from the analysis of the SNC meteorites, all predict similar amounts of Th (55–64 ppb) and U (16 ppb) but differ considerably in the K abundance (160–920 ppm). When using these models, we always obtain a similar present-day Urey ratio. On the other hand, the model of *Morgan and Anders* [1979] predicts almost twice as much Th (101 ppb) and U (28 ppb), which considerably changes the present-day value of *Ur*. However, the surface abundance of radiogenic Th and K measured by the gamma ray spectrometer on board of Mars Odyssey [*Hahn et al.*, 2011] can help discriminate between the proposed HPE models. The average K/Th ratio was found to be 5300, a value that is best consistent with the compositional model from *Wänke and Dreibus* [1994], for which this ratio is 5446. Other HPE models predict either a K/Th ratio 3 times higher, i.e., 16,727 [*Lodders and Fegley*, 1997], or very low, i.e., 2500 [*Treiman et al.*, 1986] or 614 [*Morgan and Anders*, 1979], when compared to the observed surface value.

The uncertainty δ_H with which H can be estimated from equation (1) can be easily calculated accounting for the expected accuracy of the measurements and the range over which the Urey ratio varies according to the predictions of our numerical models:

$$\delta_H = \sqrt{\left(\frac{\Delta Ur}{Ur}\right)^2 + \left(\frac{\Delta F_s}{F_s}\right)^2 + \left(\frac{\Delta M}{M}\right)^2}, \tag{10}$$

where $M = \rho_{\mathrm{sil}} V_{\mathrm{sil}}$ is the mass of the silicate fraction and ΔUr, ΔF_s, and ΔM are the uncertainties in the Urey ratio, surface heat flux, and silicate mass, respectively. Assuming that the global heat loss can be obtained from the heat flux measurement with an uncertainty of 20% [*Grott et al.*, 2007] and that the distance to a possible mantle plume is large enough that its contribution will not affect the measurement and that the InSight seismic experiment will permit to determine the silicate mass fraction of the planet to within 20%, error propagation (equation (10)) yields an uncertainty of 30% in the heat production rate. Since the bulk Urey ratio is independent on the distribution of radioactive elements between mantle and crust, the uncertainty in the heat source distribution does not contribute to the error propagation. The present-day heat

production predicted by the HPE models of *Wänke and Dreibus* [1994], *Treiman et al.* [1986], and *Lodders and Fegley* [1997] varies between 3.7 pW/kg and 6.1 pW/kg. The difference between *Wänke and Dreibus* [1994] and *Treiman et al.* [1986] models is only ∼10% and thus lies within the measurement error bars. To be able to distinguish between these two models, the uncertainty of both numerical models and measurement should lie below 6%. The model of *Lodders and Fegley* [1997], however, predicts a present-day heat production rate that is 48% higher than that obtained from the models of *Wänke and Dreibus* [1994] and *Treiman et al.* [1986]. Therefore, the InSight measurement should allow us to distinguish at least between the compositional models of *Lodders and Fegley* [1997] and *Wänke and Dreibus* [1994], or *Treiman et al.* [1986], which, albeit significantly different in their thermal evolution, lead to very similar present-day Urey ratios.

In addition, besides the possibility to distinguish between the existing HPE models, the InSight heat flux measurement may also allow us to answer the fundamental question as to whether Mars heat sources content is actually chondritic [*Phillips et al.*, 2008]. Heat flux estimates inferred from the large present-day thickness of the elastic lithosphere predicted for the north polar cap (>300 km according to *Phillips et al.* [2008]) are significantly lower (less than 15 mW/m^2) than the average values of about 21 mW/m^2 predicted both by previous parametrized thermal evolution models based on the HPE content of *Wänke and Dreibus* [1994] [*Grott and Breuer*, 2010; *Morschhauser et al.*, 2011], as well as by the models presented here. From our 3-D convection simulations, we also determined the magnitude of lateral heat flux variations caused by mantle plumes (which will be the subject of a follow-up study). Even though all models lead to the same average surface heat flux, we observed peak-to-peak variations in the thickness of the elastic lithosphere up to 130 km between upwelling and downwelling associated with models characterized by low-degree convection structures. Our highest values for the elastic lithosphere thickness are around 240–250 km, thus about 50 km thinner than the 300 km inferred for the north pole. One possible interpretation is that the HPE content of Mars' interior could be subchondritic [*Phillips et al.*, 2008]. In order to test this hypothesis with the InSight heat flux measurement, we need to require that both the ratios of Th/U and K/Th are well determined. In particular, it is necessary to assume that the K/Th ratio predicted by the gamma ray measurement reflects the ratio in the mantle source region [*Taylor et al.*, 2006]. In Figure 2d, we also show isolines of the present-day surface heat flux (dashed lines) in addition to the Urey ratio (colors and solid lines). The K/Th ratio is constant along each line passing through the origin. Assuming the K/Th ratio to be equal to the value obtained by the gamma ray measurements, any heat flux isoline intersecting the line that passes through the origin and the data point of *Wänke and Dreibus* [1994] in Figure 2d represents a possible average heat flux. Assuming that InSight will measure a low heat flux similar to the one determined below the north pole and that such a value is actually representative for Mars, our results would suggest a subchondritic content with Th = 30 ppb, K = 163.3 ppm, and U = 7.5 ppb, together with a Urey ratio which is smaller by 0.1 than the value associated with the HPE model of *Wänke and Dreibus* [1994].

These findings also emphasize the importance of deriving the average Martian heat flux from the single measurement that will be performed in the Elysium region. The planned landing site is at a distance of about 1395 km from Elysium Mons, ∼1162 km from Albor Tholus, and ∼1835 km from Hecates Tholus, volcanic centers that show their most recent activity around 3.1 Ga, 500 Ma, and 100 Ma ago, respectively [*Werner*, 2009], and can be possibly underlain by a mantle plume. Numerical models of Martian mantle convection, however, show that regions characterized by an anomalously high surface heat flux caused by upwellings have a limited spatial extent [*Plesa et al.*, 2015]. Therefore, the InSight measurement will most likely not be affected by the presence of a mantle plume. The detailed analysis of this issue will be the subject of a forthcoming study.

5. Conclusions

Under the assumption of efficient mantle cooling, our models show that the present-day Urey ratio is rather insensitive to different K abundances, but it is strongly affected by the concentration of Th and U. Using solar system values for the Th/U ratio and assuming the bulk Th abundance to be known and similar to that predicted by *Wänke and Dreibus* [1994], *Treiman et al.* [1986], or *Lodders and Fegley* [1997], the Urey ratio of Mars can be computed with an uncertainty of likely less than 10% (from 3-D simulations in spherical geometry, $Ur = 0.594 \pm 0.024$). This finding is robust and does not depend on the distribution of heat sources between mantle and crust and on the model complexity (i.e., use of Boussinesq or extended Boussinesq approximation, phase transitions, different core radii, or self-consistent treatment of crust formation and its accompanying effects). Combining this information with an estimate of the global heat loss derived from the upcoming heat flux measurement by InSight, the heat production rate H and thus the bulk abundance of heat-producing

elements in the Martian interior can be estimated. In particular, we will be able to discriminate between the HPE models of *Wänke and Dreibus* [1994] and *Treiman et al.* [1986] in comparison to that of *Lodders and Fegley* [1997]. All these models predict similar amounts of Th (55–64 ppb) and U (16 ppb) but differ considerably in the K abundance (160–920 ppm). Assuming that the ratios of Th/U and K/Th are both well known, we will also be able to answer the question as to whether Mars' HPE content is chondritic or not.

Acknowledgments

All the parameters used in the models and their outcomes are listed in Tables 1–4. All the data contained in the paper can be made available upon request from the authors. This work has been supported by the Helmholtz Association through the research alliance "Planetary Evolution and Life" and through the grant VG-NG-1017, by the Deutsche Forschungsgemeinschaft (grant TO 704/1-1), and by the Interuniversity Attraction Poles Programme initiated by the Belgian Science Policy Office through the Planet Topers alliance. Computational time has been provided by the Norddeutscher Verbund für Hoch- und Höchstleistungsrechnen (HLRN) through the project "Partial melting and the thermochemical evolution of terrestrial planets."

References

Breuer, D., and T. Spohn (2003), Early plate tectonics versus single plate tectonics on Mars: Evidence from the magnetic field history and crust evolution, *J. Geophys. Res.*, *108*(E7), 5072, doi:10.1029/2002JE001999.

Breuer, D., T. Spohn, and U. Wüllner (1993), Mantle differentiation and the crustal dichotomy of Mars, *Planet. Space Sci.*, *21*(4), 269–283.

Butler, S. L. (2009), The effects of phase boundary induced layering on the Earth's thermal history, *Geophys. J. Int.*, *179*, 1330–1340, doi:10.1111/j.1365-246X.2009.04396.x.

Christensen, U. R. (1984), Convection with pressure- and temperature-dependent non-Newtonian rheology, *Geophys. J. R. Astron. Soc.*, *77*, 343–384.

Christensen, U. R., and D. A. Yuen (1985), Layered convection induced by phase transitions, *J. Geophys. Res.*, *90*, 10,291–10,300.

Fraeman, A., and J. Korenaga (2010), The influence of mantle melting on the evolution of Mars, *Icarus*, *210*(1), 43–57, doi:10.1016/j.icarus.2010.06.030.

Grott, M., and D. Breuer (2008), The evolution of the Martian elastic lithosphere and implications for crustal and mantle rheology, *Icarus*, *193*, 503–515, doi:10.1016/j.icarus.2007.08.015.

Grott, M., and D. Breuer (2010), On the spatial variability of the Martian elastic lithosphere thickness: Evidence for mantle plumes?, *J. Geophys. Res.*, *115*, E03005, doi:10.1029/2009JE003456.

Grott, M., J. Helbert, and R. Nadalini (2007), Thermal structure of Martian soil and the measurability of the planetary heat flow, *J. Geophys. Res.*, *112*, E09004, doi:10.1029/2007JE002905.

Hahn, B. C., S. M. McLennan, and E. C. Klein (2011), Martian surface heat production and crustal heat flow from Mars Odyssey Gamma-Ray spectrometry, *Geophys. Res. Lett.*, *38*, L14203, doi:10.1029/2011GL047435.

Hauck, S. A., and R. P. Phillips (2002), Thermal and crustal evolution of Mars, *J. Geophys. Res.*, *107*(E7), 5052, doi:10.1029/2001JE001801.

Hubbard, N. J., P. W. Gast, C. Meyer, L. E. Nyquist, C. Shih, and H. Wiesmann (1971), Chemical composition of lunar anorthosites and their parent liquids, *Earth Planet. Sci. Lett.*, *13*(1), 71–75.

Hüttig, C., and K. Stemmer (2008), The spiral grid: A new approach to discretize the sphere and its application to mantle convection, *Geochem. Geophys. Geosyst.*, *9*, Q02018, doi:10.1029/2007GC001581.

Jaupart, C., and J. C. Mareschal (2007), Heat flow and thermal structure of the lithosphere, *Treatise Geophys.*, *6*, 217–252.

Jolliff, B. L., J. J. Gillis, L. A. Haskin, R. L. Korotev, and M. A. Wieczorek (2000), Major lunar crustal terranes: Surface expressions and crust-mantle origins, *J. Geophys. Res.*, *105*(E2), 4197–4216, doi:10.1029/1999JE001103.

Karato, S. I., M. S. Paterson, and J. D. F. Gerald (1986), Rheology of synthetic olivine aggregates: Influence of grain size and water, *J. Geophys. Res.*, *91*, 8151–8176.

Keller, T., and P. J. Tackley (2009), Towards self-consistent modeling of the Martian dichotomy: The influence of one-ridge convection on crustal thickness distribution, *Icarus*, *202*, 429–443.

Kiefer, W. S., and Q. Li (2009), Mantle convection controls the observed lateral variations in lithospheric thickness on present-day Mars, *Geophys. Res. Lett.*, *36*, L18203, doi:10.1029/2009GL039827.

Korenaga, J. (2006), Archean geodynamics and the thermal evolution of the Earth, in *Archean Geodynamics and Environments, Geophys. Monogr. Ser.*, vol. 164, edited by J.-C. M. K. Benn, and K. C. Condie, pp. 320, AGU, Washington, D. C.

Korenaga, J. (2008), Urey ratio and the structure and evolution of Earth's mantle, *Rev. Geophys.*, *46*, RG2007, doi:10.1029/2007RG000241.

Laneuville, M., M. A. Wieczorek, D. Breuer, and N. Tosi (2013), Asymmetric thermal evolution of the Moon, *J. Geophys. Res. Planets*, *118*, 1435–1452, doi:10.1002/jgre.20103.

Langseth, M. G., S. J. Keihm, and K. Peters (1976), Revised lunar heat-flow values, *Proc. Lunar Planet. Sci. Conf.*, *7*, 3143–3171.

Lawrence, D. J., W. C. Feldman, B. L. Barraclough, A. B. Binder, R. C. Elphic, S. Maurice, M. C. Miller, and T. H. Prettyman (2000), Thorium abundances on the lunar surface, *J. Geophys. Res.*, *105*(E8), 20,307–20,331, doi:10.1029/1999JE001177.

Lenardic, A., C. M. Cooper, and L. Moresi (2011), A note on continents and the Earth's Urey ratio, *Phys. Earth Planet. Inter.*, *188*(1-2), 127–130, doi:10.1016/j.pepi.2011.06.008.

Lodders, K., and B. Fegley (1997), An oxygen isotope model for the composition of Mars, *Icarus*, *126*(2), 373–394.

McCubbin, F. M., E. H. Hauri, S. M. Elardo, K. E. V. Kaaden, J. Wang, and C. K. Shearer (2012), Hydrous melting of the Martian mantle produced both depleted and enriched shergottites, *Geology*, *40*, 683–686, doi:10.1130/G33242.1.

Morgan, J. W., and E. Anders (1979), Chemical composition of Mars, *Geochim. Cosmochim. Acta*, *43*(10), 1601–1610, doi:10.1016/0016-7037(79)90180-7.

Morschhauser, A., M. Grott, and D. Breuer (2011), Crustal recycling, mantle dehydration, and the thermal evolution of Mars, *Icarus*, *212*, 541–558, doi:10.1016/j.icarus.2010.12.028.

Nakagawa, T., and P. J. Tackley (2012), Influence of magmatism on mantle cooling surface heat flow and Urey ratio, *Earth Planet. Sci. Lett.*, *329–330*, 1–10, doi:10.1016/j.epsl.2012.02.011.

Neumann, G. A., M. T. Zuber, M. A. Wieczorek, P. J. McGovern, F. G. Lemoine, and D. E. Smith (2004), Crustal structure of Mars from gravity and topography, *J. Geophys. Res.*, *109*, E08002, doi:10.1029/2004JE002262.

Phillips, R. J., et al. (2008), Mars north polar deposits: Stratigraphy, age, and geodynamical response, *Science*, *320*(5880), 1182–1185, doi:10.1126/science.1157546.

Plesa, A.-C. (2011), Mantle convection in a 2D spherical shell, *INFOCOMP 2011: The First International Conference on Advanced Communications and Computation,* Barcelona, Spain, pp. 167–172.

Plesa, A.-C., and D. Breuer (2014), Partial melting in one-plate planets: Implications for thermo-chemical and atmospheric evolution, *Planet. Space Sci.*, *98*, 50–65, doi:10.1016/j.pss.2013.10.007.

Plesa, A. C., N. Tosi, M. Grott, and D. Breuer (2015), How large are heat flow variations across Mars' surface?, *LPSC,* Houston, Tex.

Roberts, J. H., and S. Zhong (2006), Degree-1 convection in the Martian mantle and the origin of the hemispheric dichotomy, *J. Geophys. Res.*, *111*, E06013, doi:10.1029/2005JE002668.

Rocholl, A., and K. P. Jochum (1993), Th, U and other trace elements in carbonaceous chondrites: Implications for the terrestrial and solar-system Th/U ratios, *Earth Planet. Sci. Lett.*, *117*, 265–278.

Ruiz, J., P. J. McGovern, A. Jimenénez-Díaz, V. López, J.-P. Williams, B. C. Hahn, and R. Tejero (2011), The thermal evolution of Mars as constrained by paleo-heat flows, *Icarus*, *215*, 508–517, doi:10.1016/j.icarus.2011.07.029.

Sekhar, P., and S. D. King (2014), 3D spherical models of Martian mantle convection constrained by melting history, *Earth Planet. Sci. Lett.*, *388*, 27–37.

Siegler, M. A., and S. E. Smrekar (2014), Lunar heat flow: Regional prospective of the Apollo landing sites, *J. Geophys. Res. Planets*, *119*, 47–63, doi:10.1002/2013JE004453.

Steinbach, V., and D. Yuen (1994), Effects of depth-dependent properties on the thermal anomalies produced in flush instabilities from phase transitions, *Phys. Earth Planet. Inter.*, *86*, 165–183.

Stevenson, D. J., T. Spohn, and G. Schubert (1983), Magnetism and thermal evolution of the terrestrial planets, *Icarus*, *54*, 466–489.

Taylor, G. J., et al. (2006), Bulk composition and early differentiation of Mars, *J. Geophys. Res.*, *111*, E03S10, doi:10.1029/2005JE002645.

Toksöz, M. N., and A. T. Hsui (1978), Thermal history and evolution of Mars, *Icarus*, *34*(3), 537–547, doi:10.1016/0019-1035(78)90043-X.

Tosi, N., D. A. Yuen, N. de Koker, and R. M. Wentzcovitch (2013a), Mantle dynamics with pressure- and temperature-dependent thermal expansivity and conductivity, *Phys. Earth Planet. Inter.*, *217*, 48–58, doi:10.1016/j.pepi.2013.02.004.

Tosi, N., M. Grott, A.-C. Plesa, and D. Breuer (2013b), Thermo-chemical evolution of Mercury's interior, *J. Geophys. Res. Planets*, *118*, 2474–2487, doi:10.1002/jgre.20168.

Treiman, A. H., M. J. Drake, M.-J. Janssens, R. Wolf, and M. Ebihara (1986), Core formation in the Earth and Shergottite Parent Body (SPB): Chemical evidence from basalts, *Geochim. Cosmochim. Acta*, *50*(6), 1071–1091, doi:10.1016/0016-7037(86)90389-3.

Wänke, H., and G. Dreibus (1994), Chemistry and accretion of Mars, *Philos. Trans. R. Soc. London*, *A349*, 2134–2137.

Warren, P. H., and K. L. Rasmussen (1987), Megaregolith insulation, internal temperatures, and bulk uranium content of the Moon, *J. Geophys. Res.*, *92*(B5), 3453–3465, doi:10.1029/JB092iB05p03453.

Werner, S. C. (2009), The global Martian volcanic evolutionary history, *Icarus*, *201*, 44–68, doi:10.1016/j.icarus.2008.12.019.

Wieczorek, M. A., and R. J. Phillips (2000), The "Procellarum KREEP terrane": Implications for mare volcanism and lunar evolution, *J. Geophys. Res.*, *105*(E8), 20,417–20,430.

Wieczorek, M. A., et al. (2013), The crust of the Moon as seen by GRAIL, *Science*, *339*(6120), 671–675, doi:10.1126/science.1231530.